

AD-A056 497

COLD REGIONS RESEARCH AND ENGINEERING LAB HANOVER N H
SIMULATION OF DRIFTING SNOW IN A HYDRAULIC FLUME, (U)
JUN 78 J L WUEBBEN

F/G 8/12

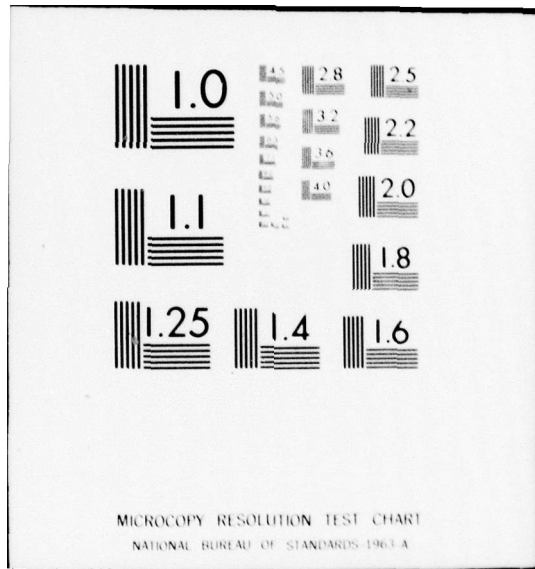
UNCLASSIFIED

NL

1 OF 1
AD
A056 497



END
DATE
FILMED
8 -78
DDC



LEVEL II



WUEBBEN

AD A 056497

ABSTRACT

11 Jun 78

6 SIMULATION OF DRIFTING SNOW IN A HYDRAULIC FLUME (U)

10 JUN 1978 JAMES L. WUEBBEN

U.S. ARMY COLD REGIONS RESEARCH AND ENGINEERING LABORATORY HANOVER, NEW HAMPSHIRE 03755

DDC RECEIVED JUL 12 1978

12 74 P1

Introduction

The objective of this investigation was to simulate conditions of drifting snow previously observed in the field in a laboratory hydraulic flume using a sand-water analog. Prototype conditions and model results were evaluated to define modeling parameters that would allow quantitative correlation between actual drift conditions and the model.

Although exact similitude is not feasible, this modeling approach has proven useful in studies of snow conditions which defy theoretical prediction and would be very time consuming or impossible to evaluate in the field. Parameters examined in the model include prototype dimensions, flow velocity, geometric scale effects, structural porosity, and time.

Past Work

ABSTRACT

Various two-phase systems have been used in the past to investigate the mechanics of blowing snow, including the sand-water analog used here. Theakston (15, 16) took a qualitative approach and developed a model which looked like blowing snow and produced drift patterns resembling those observed in the field. While largely ignoring the quantitative aspects, he was able to use the model as a practical design tool to study the effect of various structural and terrain modifications in the control of snow accumulation.

Isyumov (6), on the other hand, developed theoretical similitude relationships in a study of roof snow loads. Although he did not attempt to correlate the model results to actual field data, he was

AD NO. DDC FILE COPY

1- 78 06 09 095

DISTRIBUTION STATEMENT A Approved for public release; Distribution Unlimited

037 100

alt

WUEBBEN

able to compare quantitatively the effects of windspeed and wind orientation, roof geometry, snowfall rate and terrain roughness within the model.

Calkins (1, 2, 3) also used a similitude approach in developing models of snow accumulation around various structures. In one study, he used the model to examine possible snow control measures near aircraft instrument landing system antenna facilities in Alaska. The feasible alternatives involved structural, terrain, and site layout modifications that could not be easily addressed in the field. During a study of a radar housing constructed in North Dakota, Calkins developed quantitative relationships within the model to correlate the horizontal drift dimensions resulting from various combinations of windspeed and the geometric scale of the model.

Experimental Design

In designing a model of drifting snow, there are a variety of factors to be considered. On a qualitative basis, the particles should move by a combination of saltation and turbulent diffusion and produce a sand bed that looks like a snow field. While an ideal model would be geometrically, kinematically, and dynamically similar, exact similitude is not practical with the sand-water analog and only the more important factors may be modeled.

A basic assumption made is that drifting occurs in dry, cohesionless snow since the sand used is essentially cohesionless in water. For predicting long-term snow conditions, Isyumov and Davenport (7) suggest an integrated approach in which the physical modelings of specific drifting events are combined with statistical descriptions of meteorological conditions in a mathematical model.

The importance of modeling the wind flow regime is generally accepted. Snyder (10) suggested that complete modeling of a neutral stability atmospheric boundary layer in general terms would result from considering the following criteria:

- 1) Geometric scaling
- 2) Reynolds number scaling (viscous effects): VL/ν
- 3) Rossby number scaling (Coriolis effects): $V/L\Omega$
- 4) Peclet number scaling (heat transfer): $L\nu/k$
- 5) Densimetric Froude scaling (gravity): $V/[gL(\rho_s - \rho_w/\rho_w)]^{1/2}$

where V is flow velocity, L is a characteristic length, ν is kinematic viscosity, Ω is earth's angular velocity, k is thermal conductivity,

ACCESSION BY	<input checked="" type="checkbox"/> White Section <input type="checkbox"/> Ref Section
DTIC	
DDC	
UNANNOUNCED	
JUSTIFICATION	
Per Basic rpt.	
ET ASC, Vol. III	
DISTRIBUTION/AVAILABILITY CODES	
Doc.	AVAIL. AND/OR SPECIAL
A	

78 06 09 095

WUEBBEN

ρ is density, and g is acceleration due to gravity. The subscripts s and w denote particle and fluid characteristics respectively.

The assumption of a neutral stability atmosphere should be valid in this model, since drifting normally occurs during periods of high winds and overcast skies. For the short distances considered here, and assuming isothermal conditions during drifting, the Coriolis and heat transfer effects can be neglected.

Besides geometric scaling considerations, this leaves Reynolds and Froude similarity to be dealt with. Although it is feasible to satisfy both of these simultaneously, it is often not practical to do so. Fortunately, however, for fully developed turbulent or "rough" flow, the flow patterns become essentially independent of the Reynolds number. Most natural surfaces are aerodynamically rough even at relatively low windspeeds. A widely used criterion for determining fully rough flow was proposed by Sutton (11) using the roughness Reynolds number: $U_* z_o / \nu > 2.5$ where U_* = shear velocity, ν = kinematic viscosity, z_o = terrain roughness length, $= \epsilon/30$ (ϵ is equivalent sand roughness).

Based on the above assumptions, modeling of the earth's turbulent boundary layer might be approximated by simulation of the terrain roughness (6). This may be stated in terms of the Jensen criterion:

$$\frac{L_m}{L_p} = \frac{z_{o_m}}{z_{o_p}} \quad (1)$$

where L is a characteristic length, z_o is the terrain roughness length, and m and p denote model and prototype conditions respectively. Since the terrain roughness length z_o was not measured in the field, it will be estimated based on measurements on similar terrain. Using data cited by Isyumov (6), the prototype terrain roughness should be in the range of 0.023 m to 0.09 m. This corresponds to model roughness lengths in the range of $0.023 \text{ cm} < z_{o_m} < 0.18 \text{ cm}$ for geometric scale ratios of 1:50 and 1:100. Because of the appreciable spread in the estimate of z_o , as well as the fact that it is only an estimate, it is not possible to model the terrain roughness accurately. Indeed, there is no clear basis for using different model roughness lengths even between geometric scales of 1:50 and 1:100.

Since the roughness length measured for the bare flume bottom was only 0.001 cm, a system of artificial roughness was developed. By randomly gluing pieces of crushed rock to the flume bottom, the rough-

WUEBBEN

ness length was increased to approximately 0.084 cm. The resulting boundary layer thickness δ in the model, based on velocity profiles, was estimated to be 8 to 10 cm deep. This is sufficient to just envelop the tallest model (7.6 cm).

Evaluating the roughness Reynolds number for the lowest flow velocity used in the model (mean velocity $V_M = 28.1$ cm/sec) yields $U_* z / \nu = 18.1$, which is within the rough flow regime defining Reynolds number independence.

Now one of the major problems in using the sand-water analog must be considered. According to Mellor (9), blown snow usually consists of roughly equidimensional grains about 0.01 cm in diameter. It is apparent that it would be difficult to maintain geometric similarity for any significant scale reduction. Strict scaling would result in the very small model particles being transported in a different flow regime unless Reynolds similarity is achieved. Therefore, in order to work under the assumption of Reynolds number independence, it is necessary to distort the model with respect to particle size. Increasing the particle size reduces the significance of viscous effects relative to inertial effects, but provided that the particles used are not too large and that they still respond to the more significant aspects of the flow structure, it may still be possible to achieve adequate similitude.

Velocity scaling will now be examined. Since sand in water is being used to simulate snow in air, density effects become important and the appropriate relationship is the densimetric Froude number cited in the initial list of criteria. Equating the model and prototype Froude numbers yields $\lambda_v = 0.0534 \lambda_L^{1/2}$, which results in velocity ratios of 1:130 and 1:190 for geometric ratios of 1:50 and 1:100 respectively. The term λ denotes a ratio of model to prototype conditions. For the weighted seasonal mean wind velocity of 16.4 m/sec during drifting cited by Tabler (12) field data, the corresponding mean model velocities would be well below the threshold of movement for the sand being used ($V_{th} = 25$ cm/sec).

Since modeling based on the the densimetric Froude number is not possible, the velocity scaling will be developed based on gross particle transport and threshold of movement characteristics. According to Isyumov (6), this can be accomplished by maintaining similarity of particle terminal fall velocity W_t and of critical shear velocity U_{*t} . This may be stated in terms of model to prototype ratios as $\lambda_v = \lambda_{W_t} = \lambda_{U_{*t}}$.

WUEBBEN

The fall velocity for the sand used in the model was not measured, but for a mean sediment diameter of 0.12 cm and a shape factor corresponding to naturally worn quartz, the terminal velocity in water at 20°C would be about 1.2 cm/sec. Corresponding information for snow derived from information given by Mellor (9) gives $W_t = 0.5 + 1.0$ m/sec for a diameter on the order of 0.1 mm. This results in a velocity ratio based on terminal fall velocity in the range of $1.42 < \lambda_{w_t} < 1.83$.

Because of the statistical nature of the entrainment process, it is not possible to pinpoint a threshold of motion, and different observers would likely estimate different thresholds. But, based on observation of a uniform bed of the model sand, the mean flow velocity at the initiation of particle motion is about $V_{th} = 25$ cm/sec, which yields $U_{*t} = 1.22$ cm/sec. Taking the threshold of motion for cohesionless snow to be in the range of 21 cm/sec $< U_{*t} < 52$ cm/sec gives a velocity ratio based on the threshold of motion in the range of $1.18 < \lambda_v < 1.43$.

Depending on a combination of geometric and wind structures factors, the dominant form of snow transport may be either saltation or turbulent diffusion. Lacking prototype data, and because of the uncertainty contained in the estimates of the parameters above, a velocity scale will be selected by equating the threshold shear velocity and the fall velocity between model and field conditions. This results in the velocity ratio $\lambda_v = 1.42$.

The Model

The objective of this investigation was to simulate conditions of drifting snow and to define modeling parameters that would allow quantitative correlation between actual drift conditions and the model. Due to the complexity of the distortion in the model, it was decided to simplify this correlation by modeling a snow fence which allows a two-dimensional analysis.

The fence modeled is the standard plan snow fence designed by the Wyoming Highway Department and installed along Interstate Highway 80 in 1971. The performance of this system has been documented by the Rocky Mountain Forest and Range Experiment Station of the U.S. Forest Service (12, 13, 14). The fence is of the horizontal slat type with 50% porosity, a bottom gap of about 40 cm, and a leeward inclination of 15°. Fence heights used in the field include 1.8, 2.4, 3.2, and 3.8 m.

The testing was conducted in a hydraulic flume at CRREL. The overall length of the flume is 10.7 m, with a working length of 7.3 m.

WUEBBEN

The cross section is normally 0.91 m deep and 0.91 m wide, but for these tests the flume width was reduced to 33 cm. The flume is of the recirculating type with a gravity feed sand hopper at the upstream end.

Model Operation

A matrix of the scheme of model run conditions using the standard 50% porosity fences is given in Table 1. These fences were constructed of round metal dowel stock. In addition, runs were made using 2.4-m-high fences at $\lambda_L = 1:100$ having densities of 75 and 100%, and a 50% density fence constructed with square doweling. These additional runs were made at a mean velocity of $V_M = 50$ cm/sec and at a sand feed rate of $F_s = 2.8$ kg/min.

Table 1. Matrix of model runs.*

Scale	1:100			1:50	
Fence height	2.4 m	3.8 m	7.6 m	2.4 m	3.8 m
F_s (kg/min)	V_M (cm/sec)	V_M (cm/sec)	V_M (cm/sec)	V_M (cm/sec)	V_M (cm/sec)
1.6	30	40	40	40	
	40	50			
2.8	50	50	50	50	50
	60				
9.6	50				

* $V_M = 50$ cm/sec, $F_s = 2.8$ kg/min.

Ideally, mass flux data would be used to correlate the model results. Originally it was intended to make measurements of sediment flux and concentration profiles using an electro-optical probe, but due to the operational characteristics of the system, the results were unsatisfactory. Because this information was lacking, the model was compared internally based on an open field (no fence in place) accumulation rate for various combinations of flow velocity and sand feed rates. This accumulation rate is defined as the average sand depth D_r divided by elapsed time.

The basis for using this open field accumulation rate dD_r/dt is the assumption that the system approaches a steady state. By feeding in enough sand at the headbox so that the sediment carrying capacity of the flow is substantially exceeded, net deposition occurs in the flume. If a steady state of both horizontal flux and deposition rate

WUEBBEN

is at least approached, deposition rates should remain more or less constant with respect to distance along the flume. These accumulation rates were calibrated by running the system at various combinations of sand feed rate and water velocity. Keeping the inexactness of these relations in mind, a comparison of drift dimensions based on the reference accumulation rate dD_r/dt gives a relative indication of fence efficiency.

Time scaling in the model might also be best determined on the basis of mass flux, but this information was lacking in both the model and prototype. Alternatively defining the deposition rate ratio as $\lambda_d D_r/dt = \lambda_r/\lambda_t = \lambda_v$ yields prototype precipitation rates in the range from 33 to 150 cm/hr. These model accumulation rates correspond to abnormally high values of prototype precipitation rates since most snowfall rates in the U.S.A. would probably be under 6 cm/hr.

Moderate distortion of the precipitation rate was found to have no appreciable effect on the model, and even some of the higher model rates used here appeared to cause only slightly more uniform depth drifts. As a result, it should be possible to reduce the time scale through the use of a distorted precipitation rate. If the rate is increased too greatly, however, drift detail may be obscured and eventually may result in burying the model.

Another basis for model comparison is the saturation value of drift formation. The point at which a fence becomes saturated is subjective since it is approached asymptotically, and in a feed-type flume with net deposition occurring the drift never really stops accumulating. While it appears that there is a vertical limit to drift growth of about 1.2 H, sand continues to be deposited in the tail portion of the drift. As a result, saturation in the model was defined as the point when the fence began to submerge rapidly. Ordinarily the fence would remain relatively clear through most of the run and then the bottom gap would plug and the fence would rapidly submerge. Whether this is the best definition of model saturation or not, it unquestionably signalled the end of a run.

Results

As a first step in evaluation of the model, the results of the various model runs will be correlated internally, and in addition qualitative comparisons will be made to conditions observed in the field. Later, the quantitative correlation of the model results to prototype data will be examined.

WUEBBEN

Velocity

The data from a series of runs using the 2.4-m at 1:100 scale model demonstrate the influence of velocity on snowdrift formation. Figure 1 gives a plot of dimensionless area A/H^2 versus the reference sand accumulation depth D_r/H . Since this relationship reflects a form of fence efficiency, when differentiated with time it indicates that the trap efficiency of the fence increases with velocity in the range of $30 \text{ cm/sec} < V_M < 50 \text{ cm/sec}$, but by $V_M = 60 \text{ cm/sec}$ the trend reverses. An examination of the data for drift length and maximum depth shows a similar trend.

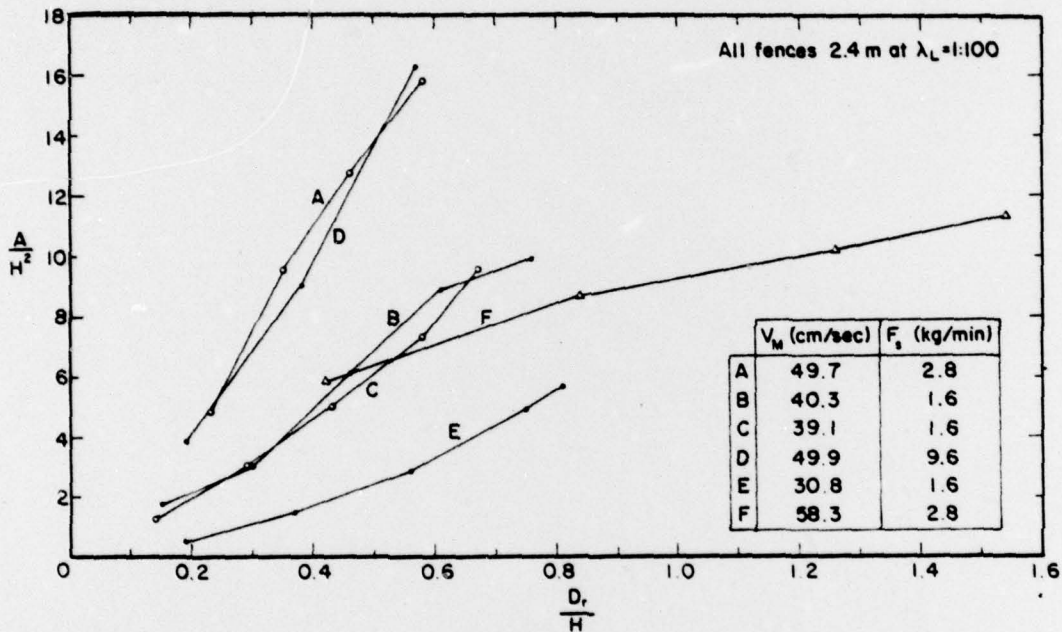


Figure 1. Influence of velocity on fence efficiency.

Examining the dimensions of the drifts for equivalent areas A/H^2 , however, shows that as velocity increases, the drift increases in length and becomes shallower. At $V_M = 60 \text{ cm/sec}$, the drift becomes both shorter and shallower by approaching a more uniform depth. The dimensions of the leeward drift at saturation for various flow rates are given in Table 2. The term X_{MAX} denotes the distance from the base of the fence to the point of maximum drift depth D_{MAX} , and X_{END} denotes the distance from the base of the fence to the tail of the drift.

WUEBBEN

Table 2. Variation in drift dimensions with flow velocity (saturation values).*

V_M (cm/sec)	D_{MAX}/H	X_{MAX}/H	X_{END}/H	A/H^2
30	1.19	2.5	8.7	6
40	1.19	3.0	24.0	10
50	1.19	3.55	24.2	16
60	0.93	4.0	26.0	11

* $H = 2.4$ m, $\lambda_L = 1:100$.

Finney (4,5) in his wind tunnel studies, concluded that the length of the eddy area produced by a vertical barrier varies directly with fence height but is independent of wind velocity. However, he noted that the distance from the fence to the position of maximum drift depth is related to windspeed. Kungurtsev (8), on the other hand, claimed evidence of an increase in a drift length with windspeed, and further postulated a linear relationship between drift length and velocity. Finally, Mellor (9) cited data by Nokkentved that indicated a shortening of the drift as velocity increased.

The data from the present study indicate that, for equal drift volumes, the length of the drift increases as velocity increases from the threshold of motion, reaches a somewhat stable value in the range of 40 to 50 cm/sec, and begins to decrease by 60 cm/sec. This would correspond to the prototype drift length increasing with wind velocity up to $V_W = 17$ m/sec and starting to decrease with increasing velocity somewhere in the range of 21 to 25 m/sec. Thus, all three trends mentioned in the literature were observed in the model depending on the velocity range.

Figure 1 also shows that two runs at $V_M = 50$ cm/sec, which are identical except for sand*feed rate, agree very well. This tends to support the contention that precipitation rate is not a dominant factor controlling the characteristics of drift development, an assumption critical to the use of an abnormally high precipitation rate ratio to reduce the time ratio. Data from the runs using the 3.8-m at $\lambda_L = 1:100$ fence also support this contention. The drifts do develop more rapidly, however, and there is a tendency towards more uniform depth as the deposition rate increases.

Fence Height

Data in which flow velocity and the sand feed rate are held constant show the expected trend of storage volume increasing with fence

WUEBBEN

height. However, the 3.8-m at $\lambda_L = 1:50$ fence produced a larger drift than the 7.6-m at $\lambda_L = 1:100$ fence even though both fences have the same physical height. This difference is attributed to the combined effects of an increased bottom gap and wider openings between slats. In the field, porosity is often considered to be the significant variable rather than slat opening and width, but because of the particle size distortion this may not be true in the model.

The maximum depths obtained for various fence heights became stable before saturation and yielded the values shown in Table 3. These data show that, as fence height increases, the drift becomes relatively shallower and longer, and has its center mass closer to the fence. These effects were not evident in the field data, however, and it is felt that the problem lies in the modeling of the boundary layer. Although the models were contained within the logarithmic portion of the velocity profile, the boundary layer thickness was not modeled, and the height of the largest model fences used approaches the thickness of the boundary layer.

Table 3. Variation in drift dimensions with fence height (saturation values).*

H_p (m)	H_m (cm)	λ_L	D_{MAX}/H	X_{MAX}/H	X_{END}/H
2.4	2.4	1:100	1.19	3.55	24.2
3.8	3.8		1.14	2.7	27.8
7.6	7.6		0.77	1.9	33.4
2.4	4.8	1:50	1.07	3.3	18.7
3.8	7.6		0.64	1.6	30.5

* $V_M = 50$ cm/sec, $F_s = 2.8$ kg/min.

Porosity

Another parameter to be examined is fence porosity. Although it is possible to geometrically model the fence porosity, the distortion present in the model makes correlation impossible with the data available.

Runs were made, however, to determine the model's relative response to porosity. Fences were constructed at geometric scales of 1:100 representing a 2.4-m fence having densities of 50, 75, and 100%. In addition, a model was constructed using square doweling to investigate the effect of slat shape.

WUEBBEN

There is a clear relationship between volumetric accumulation and porosity. At least for porosities less than 50% as studied here, the fence storage efficiency increases as porosity decreases. The effective porosity of the square doweled fence is between 0 and 25%, even though its geometric shadow porosity is 37% and its porosity when not inclined is 50%. This indicates that that shape of the dowels is significant.

The dimensions of the leeward drift at saturation for the various porosity runs are listed in Table 4. Although there is no large difference in the maximum drift depth, the distance from the fence to the position of maximum depth varies greatly. Also, the solid fence produced the longest drift; this is contrary to conditions observed in the field.

Table 4. Variation of drift dimensions with fence porosity* (saturation values).

Porosity (%)	D_{MAX}/H	X_{MAX}/H	X_{END}/H	A/H^2
0	1.22	9.2	35.8	24.0
25	1.2	5.5	24.0	17.5
50	1.19	3.3	24.2	16.0
37+	1.25	4.9	27.0	17.6

* $V_M = 50$ cm/sec, $F_s = 2.8$ kg/min.

+Geometric shadow porosity, square doweled.

Model Correlation

From the data discussed in the previous section, it was possible to develop a relationship that would predict the unit storage volume (or cross-sectional area of the drift) at any time, based on the fence height, flow velocity and sand feed rate. This was accomplished by assuming a linear relationship for the central portions of the A/H^2 vs D_r/H plots found in Figure 1. It was further determined that the variation in these relationships due to the velocity was essentially logarithmic in nature. Combining these two trends yields the following relationship:

$$\frac{A}{H^2} = \frac{D_r t}{tH} \times 10^{0.027 V_M + 0.162} - 2.4 \quad (2)$$

Equation 2 was evaluated by comparing measured values to those predicted by the equation. Evaluation of data for different fence heights and velocities showed an error of less than 10% for almost all data except those at the lowest values of A/H^2 . However, in view of

WUEBBEN

the inherent inaccuracy of using an open field deposition rate as an indication of sand flux, this relationship appears reasonable.

It was also possible to predict the variation in the distance from the fence to the point of maximum depth of drift. The relationship appears to be linear, at least in the range of $30 < V_M < 60$ cm/sec. Because of sparse data, the variation with fence height was not evaluated, but for the 2.4-m fence at $\lambda_L = 1:100$, the variation X_{MAX} with mean velocity may be described as

$$\frac{X_{MAX}}{H} = 0.054 V_M + 0.86 \quad (3)$$

where V_M is in units of cm/sec.

The maximum drift depth (D_{MAX}/H) varied with fence height, but no definable relationship was evident. The shortest fences, however, showed more consistent drift depths and, therefore, velocity independence. Although the models were maintained within the logarithmic portion of the velocity profiles, the taller fences were nearly as tall as the boundary layer thickness. The shorter fences, which performed better, more nearly approached the prototype boundary layer proportions. Table 2 listed the relative dimensions for the 2.4-m at $\lambda_L = 1:100$ fence, which will be used in further analysis since it is the best documented fence and apparently gave the best results.

An examination of Table 2 shows that the results of the 2.4-m fence are quite similar to the prototype data, except that the cross-sectional area of the drift is slightly smaller and closer to the fence than that of the prototype. Based on the data with the porosity runs and considering the effect of constructing the models from round doweling, it appears that the 2.4-m fence at a geometric scale of 1:100 with a nominal porosity of 25% best represents the field data. This is dubious supposition at best, however, since there are insufficient data to quantitatively evaluate the influence of porosity in this distorted model. Table 5 compares the characteristic prototype drift dimensions with those of the model 2.4-m fences at a geometric scale of 1:100 and porosities of 25 and 50%.

Table 5. Comparison of model and prototype data at saturation.

Fence	D_{MAX}/H	X_{MAX}/H	X_{END}/H	A/H^2
Prototype	1.2	5.7	24.0	18.0
Model 25% porosity	1.2	5.5	24.0	17.5
Model 50% porosity	1.22	3.3	24.2	16.0

WUEBBEN

In examining the formation of the model drifts relative to the field data, difficulties were encountered, since useful flux measurements were not obtained in the field either. Although a flux gage was installed, it was used more to record the occurrence rather than the magnitude, of drifting. However, it is interesting to note the similarity of drift formation in the model and prototype. In both cases the drift approaches its maximum depth rapidly and then the tail of the drift continues to build.

If the 2.4-m fence at $\lambda_L = 1:100$ were taken as a reasonable simulation, the corresponding windspeed would be in the range of $17 \text{ m/sec} < V_w < 25 \text{ m/sec}$. This would be a reasonable velocity range since, according to Tabler's field data (12), windspeeds greater than 17.5 m/sec occurred during more than 45% of the drifting events, and in fact the mean windspeed during the drifting was 16.4 m/sec . This suggests the concept of a "significant wind" in modeling, that is, a windspeed that is high enough to form the snowdrifts observed in the field and that occurs frequently enough to significantly influence the drift development.

Summary and Conclusions

Although problems with the inadequate modeling of the atmospheric boundary layer were encountered, it was possible to find reasonable quantitative relationships between the results from different model conditions, and a tentative correlation between these results and the prototype data. Specific conclusions from the study are:

1. The modeling of drifting snow using a distorted sand-water analogy appears useful on a practical basis. Because of insufficient prototype and sand flux data, however, some assumptions made are tenuous.
2. The simulation of the atmospheric boundary layer is of primary importance. This may take the form of modeling the terrain roughness and boundary layer thickness. While accurate modeling of the boundary layer thickness may not be possible, the model structure should at least be small in comparison ($H_m \ll \delta_m$).
3. With geometric scaling based on the terrain roughness and boundary layer thickness, velocity scaling based on particle fall velocity and threshold of motion characteristics yields good correlation between model and prototype data.
4. Similarity of the precipitation rate is not essential, and an abnormally high rate may be used in the model to reduce the time

WUEBBEN

scaling. As the precipitation rate is increased, however, there is a tendency to obscure detail of the model.

5. The response of the model to porosity and dowel shape is significant, indicating a need for detailed model construction.

Literature Cited

1. Calkins, D. (1974) Model studies of drifting snow patterns at Safeguard facilities in North Dakota. USA CRREL Technical Report 256. AD A006018.
2. Calkins, D. (1975) Simulated snowdrift patterns: Evaluation of geometric modeling criteria for a three-dimensional structure. USA CRREL Special Report 219. AD 007735.
3. Calkins, D. (1976) Evaluation and recommendations for snowdrift control at FAA ILS facilities, Barrow and Deadhorse, Alaska. U.S. Department of Transportation, Federal Aviation Administration Report No. FAA-RD-76-139.
4. Finney, E.A. (1934) Snow control on the highway. Michigan State College, Experiment Station Bulletin no. 57.
5. Finney, E.A. (1939) Snow drift control by highway design. Michigan State College Engineering Experiment Station Bulletin no. 86.
6. Isyumov, N. (1971) An approach to the prediction of snow loads. Ph.D. Dissertation to the Faculty of Engineering Science, The University of Western Ontario, London, Ontario, Canada.
7. Isyumov, N. and A.G. Davenport (1974) A probabilistic approach to the prediction of snow loads. Canadian Journal of Civil Engineering, vol. 1, no. 28.
8. Kungurtsev, A.A. (1956) The transfer and deposit of snow. Institut Geografii Akad Nauk SSSR. USA CRREL Draft Translation. (Unpublished).
9. Mellor, M. (1965) Blowing snow. USA CRREL Cold Regions Science and Engineering Monograph III-A3c. AD 630328.
10. Snyder, W. (1972) Similarity criteria for the application of fluid models to the study of air pollution meteorology. Boundary Layer Meteorology, vol. 3, no. 1, Sept, p. 113-134.